Dynamics of a polymer in a Brownian ratchet

James M. Polson,[1] Brian Bylhouwer,[1] Martin J. Zuckermann,[2] Arthur J. Horton,[1] and William M. Scott[1]
[1]*Department of Physics, University of Prince Edward Island, Charlottetown, Prince Edward Island, Canada C1A 4P3*
[2]*Department of Physics and IRMACS, Simon Fraser University, Burnaby, British Columbia, Canada V5A 1S6*
(Received 10 March 2010; revised manuscript received 29 September 2010; published 30 November 2010)

We have used Brownian dynamics simulations to study the dynamics of a bead-and-spring polymer subject to a flashing ratchet potential. To elucidate the role of hydrodynamic (HD) interactions, simulations were carried out for the cases where HD interactions are present and when they are absent. The average speed of the polymer and its conformational properties were examined upon variation in the polymer length, N, and the ratchet spatial period, L. Two distinct dynamical regimes were evident. In the low-N/high-L regime, the velocity decreases with increasing N, and center-of-mass diffusion is a key part of the motional mechanism. By contrast, in the high-N/low-L regime, the velocity is insensitive to variation in N, and motion is achieved via the coupling of internal modes to the cycling of the ratchet potential. The location of the regimes is correlated with the average conformational state of the polymer. Incorporating HD interactions increases the average polymer velocity for all polymer lengths and ratchet spatial periods considered. The dynamical behavior of polymers in the low-N/high-L regime can be understood using simple a theoretical model that yields quantitatively reasonable predictions of the polymer velocity.

DOI: 10.1103/PhysRevE.82.051931 PACS number(s): 87.15.ap, 87.15.H−, 05.40.−a, 05.60.Cd

I. INTRODUCTION

Molecular separation methods based on transport are often used for the size-based separation of DNA fragments of varying lengths. Many of these procedures employ disordered nanoporous materials such as polymeric gels and fibrous membranes or artificial nanostructures as molecular sieves or filters. Separation arises from the sensitivity of the molecular mobility to the relative size of the molecule to the mean pore size of the matrix [1–3]. The natural limitations of such approaches have motivated the development of other methods for molecular transport and separation. One such method uses the concept of a Brownian ratchet and was investigated experimentally by Bader *et al.* [4–6] a decade ago. These authors constructed a device composed of a system of parallel microelectrodes of alternating charge that were asymmetrically positioned on a silicon substrate. By cyclically charging and discharging the electrodes, the Brownian motion of charged molecules can be rectified, and transport can be achieved. This device was used to transport strands of ssDNA of length 20–100 nt, and the resultant data were found to be in partial agreement with theoretical predictions using a simple model. For the electrode dimensions and ssDNA lengths employed, the transport rate was determined primarily by the rate of diffusion, which in turn is dependent on molecular size. Consequently, this type of device, in principle, can be used for the transport and size-based separation of DNA and other biopolymers such as charged proteins.

The purpose of the present study is to use computer simulation methods to investigate fully the transport and thermodynamic properties of devices of the type studied in Refs. [4–6] for polymers. We employ a simple bead-spring description of the polymer and model the polymer-electrode interaction using a one-dimensional (1D) spatially asymmetric external potential. This work builds on other recent simulation studies that used comparable models [7–9]. We focus primarily on the effects of hydrodynamic (HD) interactions on the transport properties, as well as coupling of the mode of transport to the average conformational state of the polymer.

In order to understand the results of simulation studies of polymer/ratchet systems, it is helpful to first review the concept of a Brownian ratchet using the ratchet model employed in this study and in Refs. [7–9] as an illustration. In this model, each monomer experiences an external potential of the form illustrated in Fig. 1. In the context of the device described in Refs. [4–6], the minima and maxima positions can be viewed as the locations of positively and negatively charged electrodes with which the negatively charged DNA fragments interact. The sawtooth form of the potential is chosen for simplicity. The potential is characterized by an amplitude, V_0, a spatial period L, and an asymmetry parameter α. In addition, the potential is toggled on and off cyclically with a period $\tau=t_{on}+t_{off}$, where t_{on} and t_{off} are the times during which the potential is turned on and off, respectively. If $V_0 \gg k_B T$, a particle subjected to this potential will be trapped in a region near a potential minimum. When the potential is off, the particles freely diffuse within the solvent with no preferred direction. At the end of the off-time, the potential is reapplied to the system, causing some of the particles to be forced toward the potential minimum to the

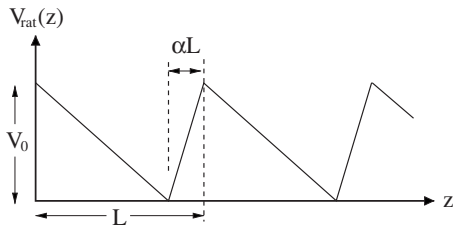

FIG. 1. Ratchet potential of Eq. (6), illustrating the potential amplitude, V_0, ratchet spatial period, L, and ratchet potential asymmetry, α.

right and a smaller number to move to the minimum to the left, while the rest return to the initial minimum. Thus, during one on/off cycle, the average particle position advances in the $+z$ direction, and repeatedly flashing the asymmetric potential on and off will result in a nonzero average or "drift" velocity of the particles. The magnitude and direction of the drift velocity can be changed by adjusting the values of the parameters of the potential. Note that the diffusion rate determines the characteristic distance traveled by the particle during the off-time and, consequently, will also affect the drift speed.

The transport mechanism described above is known as a "flashing ratchet" and is one of many types of Brownian ratchets. More generally, Brownian ratchets are systems in which the Brownian motion of diffusive particles is rectified by breaking the symmetry of the system and forcing it from equilibrium. Other examples of symmetry breaking include rocking ratchets [10] and the use of thermal oscillations [11,12]. Brownian ratchet systems of this type have been studied in detail both experimentally [4–6,13–21] and theoretically [7–10,22–37] in recent years and have served as theoretical models for biological and synthetic molecular motors [7,26–28,38–41].

Downton *et al.* used Langevin dynamics simulations to study the transport of a flexible bead-and-spring polymer subject to a flashing ratchet using the potential illustrated in Fig. 1 [7,8]. For simplicity, HD interactions were omitted. The drift velocity was characterized as a function of L, t_{off} and the number of monomers per polymer, N, and the ratchet performance was characterized using several measures, including the Peclet number to quantify the coherency, the rectification efficiency and stall force. One notable result was the fact that the drift velocity remained relatively constant with respect to variations in N for the range of polymer lengths investigated ($25<N<500$). Since the diffusion coefficient, D, of the polymer is strongly dependent on N ($D \propto 1/N$ in the absence of HD), it was concluded that center-of-mass diffusion is not an important part of the motional mechanism. An analysis of the Rouse coordinates revealed the mechanism instead relies more on the coupling of the internal modes of motion to the ratchet cycling. This picture also accounted for the observation that the polymer was able to transport a load without suffering a significant drop in drift velocity.

Kenward and Slater studied the behavior of a polymer/ratchet system using molecular dynamics simulations [9]. While they used the same polymer model and ratchet potential as that used in Ref. [8], their model also included an explicitly modeled solvent, thereby enabling the observation of HD effects. They found that a shape deformation induced by the ratchet potential during the on-time of the ratchet cycle influences the transport rate of the polymer. During the off-time the polymer relaxes from a deformed oblate shape to its equilibrium spherical shape, and this shape anisotropy relaxation leads to a time-dependent diffusion coefficient, which can have an appreciable effect on the drift velocity. This effect is a result of HD interactions and is not present for the model employed in Ref. [8]. The authors also analyzed their results using a modified version of the theory employed to analyze the experimental data in Refs. [4–6].

In this study we seek to better characterize and understand the transport behavior of polymers in flashing ratchets. The insensitivity of the drift velocity to polymer length observed in Refs. [7,8] apparently suggests that a device employing the flashing ratchet mechanism might not be effective as a transport-based separation procedure for polymers, as envisaged by Bader *et al.* However, it should be noted that the simulations were carried out in cases where the polymer dimensions were comparable L. In the case where the polymer size is small relative to L, center-of-mass diffusion is expected to be more a significant part of the transport mechanism; consequently, the drift speed should exhibit greater sensitivity to variations in N. One of the goals of this study is to expand the parameter range to explore and quantify the crossover between the two dynamical regimes. Another goal is motivated by the results of Ref. [9], which highlight the importance of HD effects, which were absent in Refs. [7,8]. HD interactions affect both the diffusion rate and the internal relaxation rate and are therefore expected to affect the polymer drift velocity in the ratchet. Consequently, in this study we also investigate the effects of HD interactions on the transport. To achieve this goal, we extend the Brownian ratchet model of Downton *et al.* [7,8] by including HD interactions using the diffusion tensor derived by Rotne, Prager, and Yamakawa (RPY) [42,43]. This is more computationally efficient than the explicit solvent MD method used in Ref. [9], thus facilitating an exploration of polymer transport over a wide range of values of system parameters. In addition, this approach enables us to compare the properties of the system both in the presence and absence of HD interactions. Simulation generated comparisons of HD effects versus their absence have recently been examined for Brownian ratchet models by Houtman *et al.* [44] and Fornés [45] for active mass transport and dimers moving against an external load, respectively.

The paper is organized as follows. The model for the polymer and flashing ratchet potential and the simulation procedure are presented in detail in Sec. II. The results of the simulations are presented and discussed in Sec. III. We show that the trends in the variation in the drift velocity and the conformational behavior with N, L, and t_{off} are consistent with the presence of two identifiable dynamical regimes, each with a distinct motional mechanism. HD interactions are shown to increase the drift speed in both regimes but for different reasons. The ratchet-induced deformation effect observed in Ref. [9] is observed in simulations with HD. We develop a simple theoretical model that yields quantitatively accurate predictions for the drift velocity in the diffusion-dominated regime. The paper is concluded in Sec. IV with a summary and some suggestions for future work.

II. MODEL AND METHOD

The model polymer is a bound chain of N spherical monomers. The ith monomer is subject to a conservative force given by $\vec{F}_i=-\vec{\nabla}_i U_{\mathrm{tot}}(\vec{r}_1,\vec{r}_2,\ldots,\vec{r}_N)$, where the total potential energy, U_{tot}, is given by

$$U_{\text{tot}} = \sum_{i<j}^{N} U_{\text{nb}}(r_{ij}) + \sum_{i=1}^{N-1} U_{\text{b}}(r_{i,i+1}) + \sum_{i=1}^{N} V_{\text{ext}}(\vec{r}_i,t). \quad (1)$$

Here, $U_{\text{nb}}(r_{ij})$ is the interaction between nonbonded monomers i and j separated by a distance r_{ij}, $U_{\text{b}}(r_{i,i+1})$ is the bonding interaction between adjacent monomers i and $i+1$, and $V_{\text{ext}}(\vec{r}_i,t)$ is the time-dependent external potential of the ratchet motor acting on monomer i. Nonbonded interactions are given by the repulsive Lennard-Jones potential

$$U_{\text{nb}}(r) = \begin{cases} U_{\text{LJ}}(r) - U_{\text{LJ}}(r_{\text{c}}), & r \le r_{\text{c}} \\ 0, & r \ge r_{\text{c}}, \end{cases} \quad (2)$$

where

$$U_{\text{LJ}}(r) = 4\epsilon\left[\left(\frac{\sigma}{r}\right)^{12} - \left(\frac{\sigma}{r}\right)^{6}\right] \quad (3)$$

and where $r_{\text{c}} \equiv 2^{1/6}\sigma$. The bonding interaction between adjacent pairs of monomers given by

$$U_{\text{b}}(r) = \frac{1}{2}k(r-\sigma)^2, \quad (4)$$

where we choose $k\sigma^2/\epsilon = 500$. The time-dependent external potential, $V_{\text{ext}}(\vec{r},t)$ has the form

$$V_{\text{ext}}(\vec{r},t) = g(t)V_{\text{rat}}(z). \quad (5)$$

The function $g(t)$ is a periodic function that toggles between a value of $g=1$ for a time t_{on} and $g=0$ for a time t_{off}. The ratchet period, τ, is simply $\tau = t_{\text{on}} + t_{\text{off}}$. Furthermore, $V_{\text{rat}}(z)$, is a piecewise linear, sawtooth potential characterized by a periodic length, L, an amplitude, V_0, and an asymmetry, α, and is defined

$$V_{\text{rat}}(z) = \begin{cases} -V_0 z/((1-\alpha)L) + V_0, & 0 < z \le (1-\alpha)L \\ V_0 z/(\alpha L) - V_0(1-\alpha)/\alpha, & (1-\alpha)L < z < L \end{cases} \quad (6)$$

and by the fact that $V_{\text{rat}}(z+L) = V_{\text{rat}}(z)$. This function is illustrated in Fig. 1. Unless otherwise indicated, $V_0 = 4k_{\text{B}}T$ and $\alpha = 0.1$ for all of the calculations presented in this paper.

The polymer motion is governed by the generalized Langevin equation:

$$\frac{d\vec{r}_i}{dt} = \sum_{j=1}^{N} \vec{\vec{\mu}}_{ij} \cdot (\vec{F}_j + \vec{f}_j), \quad (7)$$

where $\vec{r}_i(t)$ is the position of the ith monomer. HD interactions are incorporated via the Rotne-Prager-Yamakawa diffusion tensor, $\vec{\vec{\mu}}_{ij}$, which is given by [42,43]

$$\vec{\vec{\mu}}_{ij} = \begin{cases} \dfrac{\vec{\vec{1}}}{6\pi\eta R}, & i = j \\ \dfrac{1}{8\pi\eta r_{ij}}\left[\left(\dfrac{2R^2}{r_{ij}^2} + \dfrac{1}{3}\right)\vec{\vec{1}} + \left(1 - \dfrac{2R^2}{r_{ij}^2}\right)\hat{r}_{ij} \otimes \hat{r}_{ij}\right], & i \ne j \text{ and } r_{ij} \ge 2R \\ \dfrac{1}{6\pi\eta R}\left[\left(1 - \dfrac{9r_{ij}}{32R}\right)\vec{\vec{1}} + \dfrac{3r_{ij}}{32R}\hat{r}_{ij} \otimes \hat{r}_{ij}\right], & i \ne j \text{ and } r_{ij} < 2R, \end{cases} \quad (8)$$

where η is the viscosity of the solvent, R $(=\sigma/2)$ is the Stokes radius of the monomer, and r_{ij} and $\hat{r}_{ij}$ are the distances and relative displacement directions, respectively, between monomers i and j. Furthermore, $\vec{F}_j = \vec{F}_j(\vec{r}_1, \ldots, \vec{r}_N)$ is the conservative force associated with the potential of Eq. (1), and $\vec{f}_i(t)$ is a stochastic variable that satisfies

$$\langle \vec{f}_i(t) \cdot \vec{f}_j(t') \rangle = 6\gamma_0 kT\delta_{ij}\delta(t-t'), \quad (9)$$

where the monomer friction coefficient, γ_0, is given by the Stokes relation, $\gamma_0 = 6\eta\pi R$.

The first-order Ermak and McCammon algorithm [46] is used to integrate Eq. (7):

$$\vec{r}_i(t+\Delta t) = \vec{r}_i(t) + \sum_{j=1}^{N} \vec{\vec{\mu}}_{ij} \cdot \vec{F}_j \Delta t + \vec{\rho}_i, \quad (10)$$

where $\vec{\rho}_i$ is a random displacement with zero mean and satisfies

$$\langle \vec{\rho}_i \otimes \vec{\rho}_j \rangle = 2\vec{\vec{\mu}}_{ij}k_{\text{B}}T\Delta t. \quad (11)$$

In the absence of HD interactions, the diffusion tensor reduces to the simplified form $\vec{\vec{\mu}}_{ij} = \vec{\vec{1}}\delta_{ij}/(6\pi\eta R)$, and the equation of motion reduces to that of the overdamped case of the Langevin equation:

$$\gamma_0 \frac{d\vec{r}_i}{dt} = \vec{F}_i(\{\vec{r}_j(t)\}_j) + \vec{f}_i(t). \quad (12)$$

All calculations were carried out at a temperature of $k_B T/\epsilon = 1$. All quantities in Sec. III are presented using the following reduced units: distances are in units of σ, energy is in units of $\epsilon = k_B T$, and time is in units of $\gamma_0\sigma^2/k_B T = \gamma_0\sigma^2/\epsilon$. The reduced units for other quantities follow from these choices.

In order to maximize computational efficiency, many separate simulations for a system with a given set of physical

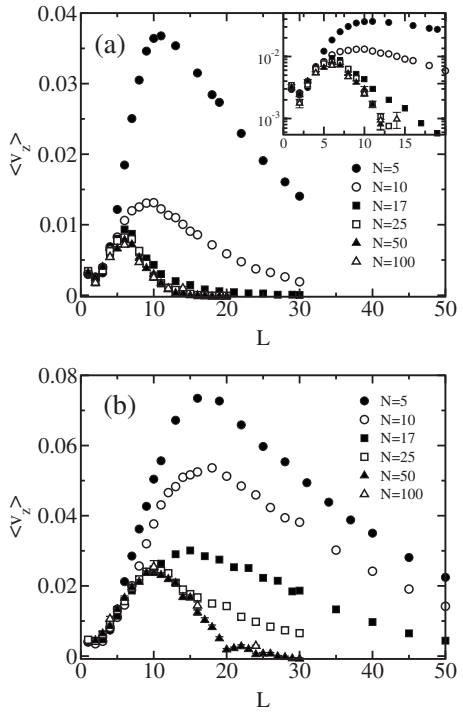

FIG. 2. (a) Polymer center-of-mass average velocity, $\langle v_z \rangle$, vs ratchet spatial period, L, for several different polymer chain lengths. The data correspond to a model system where HD interactions are *absent*. The inset shows a close-up of the same data on a semilogarithmic scale. (b) As in (a), except for a system in which HD interactions are *present*. In all cases, $t_{\mathrm{off}}=t_{\mathrm{on}}=20$, $V=4$, and $\alpha=0.1$.

parameter values were run on separate processors, each using a distinct sequence of random numbers. Consequently, the simulations were statistically uncorrelated, and the results obtained from the parallel runs were gathered together and analyzed as a single set. The chosen number of parallel simulations and the time range for each system varied, depending on the polymer length and on whether HD interactions were present. (Simulations of systems with HD interactions tend were more time consuming that those without HD systems, especially for longer chain lengths.) For example, for $N=50$ polymers with HD interactions there were 160 separate simulations each of duration $\Delta t_{\mathrm{max}}=20\,000$. Finally, all simulations employed a time step of $\Delta t=0.0001$

III. RESULTS AND DISCUSSION

A. Drift velocity

Figure 2 shows the measured values of the average velocity of the polymer, $\langle v_z \rangle$, as a function of the ratchet spatial period, L, for polymer lengths in the range $N=5-100$. Results for a polymer in the absence of HD interactions are shown in Fig. 2(a), and results for a polymer where HD interactions are present are shown in Fig. 2(b). One consistent qualitative trend stands out: for each polymer length, N, $\langle v_z \rangle$ consistently exhibits a single maximum at some optimal ratchet period, regardless of whether HD interactions are present or absent. This behavior is qualitatively consistent with the expectation that the $\langle v_z \rangle \to 0$ in the limits of small and large L. In addition, there are several other trends in the data whose significance we discuss below.

Consider first the non-HD results of Fig. 2(a). These data are quantitatively consistent with the drift velocities reported in Ref. [8] for the range of chain lengths ($N \geq 25$) considered in that study, with the exception of a minor quantitative difference that arises from employing a slightly different model and numerical integration method in the present study [47]. The key point noted in Ref. [8] was the extremely weak dependence of $\langle v_z \rangle$ on N. Since the polymer diffusion coefficient is strongly dependent on N ($D \propto N^{-1}$, in the absence of HD interactions), Downton *et al.* concluded that the mode of transport for the polymer is not the same as that of a traditional flashing ratchet, which relies on center-of-mass diffusion. It was suggested, rather, that the dominant driving mechanism involves the coupling of the internal dynamics of the polymer to the flashing ratchet, though a detailed theoretical analysis was not presented. However, it is evident from Fig. 2(a) that this conclusion is not valid for all values of N and L. For polymer lengths in the range $N<25$ (especially $N=5$ and 10), $\langle v_z \rangle$ increases with decreasing N, a trend that *is* qualitatively consistent with a driving mechanism dependent on center-of-mass diffusion. Inspection of a close-up of the data shown in the insert of the figure provides a clearer picture the trends in the data. It appears that each $\langle v_z \rangle$ vs L curve converges with the others at sufficiently low L. This is clearly evident in the cases of $N=5$, 10, and 17. The L value of the convergence point increases with increasing N. For example, $L \approx 4$ for $N=5$, $L \approx 5$ for $N=10$, and $L \approx 7$ for $N=17$. It is likely that the trend continues for the data for higher N but is masked by statistical uncertainties.

The results for the HD system in Fig. 2(b) display a number of similarities and differences relative to those for the non-HD system in Fig. 2(a). One notable quantitative difference is the fact that $\langle v_z \rangle$ is greater when HD interactions are incorporated into the model. This is a consistent pattern, independent of N or L for the range of values considered. In addition, the location of the maximum velocity for a specific N shifts to higher values when HD interactions are present. In spite of these differences, other trends are similar. Most notably, as in Fig. 2(a), there exists a regime corresponding to high N and low L in which $\langle v_z \rangle$ is invariant to changes in N, and another regime of low N and high L in which $\langle v_z \rangle$ increases monotonically with decreasing N. As in the non-HD case, the regime boundary is determined from the values of L at which the velocity curve for a given N first diverges from the others corresponding to higher N. For example, $\langle v_z \rangle$ is insensitive to variations in N at $N>5$ for $L \approx 4$, $N>10$ for $L \approx 7$, $N>17$ for $L \approx 10$, and $N>25$ for $L \approx 15$.

These results suggest that there are at least two different parameters regimes: (1) a high-N/low-L regime where $\langle v_z \rangle$ is invariant to changes in N and L and where center-of-mass diffusion is not the important for polymer transport and (2) a low-N/high-L regime where $\langle v_z \rangle$ is sensitive to changes in N and L and where center-of-mass diffusion plays is a significant part of the transport mechanism. The values of N and L at which the system crosses from one regime to the other are clearly affected by the presence of HD interactions. In either regime, HD interactions increase the drift velocity of the polymer.

B. Ratchet-induced shape deformation of the polymer

To better quantify and understand the two regimes introduced above, let us examine the variation of the polymer conformational behavior with L and N. As noted previously, [9] the average size and shape of a free polymer will be distorted when subjected to an external potential such as the ratchet potential of Eq. (6). The deformation will undergo cyclic variations as the potential is toggled on and off. To quantify the shape deformation, we introduce the deformation factor β_z, which is defined

$$\beta_z \equiv \langle R_z^2 \rangle / \langle R_z^2 \rangle_{\text{eq}}, \tag{13}$$

where

$$R_z^2 = \frac{1}{N} \sum_{n=1}^{N} (z_n - z_{\text{cm}})^2 \tag{14}$$

and where z_n and z_{cm} are the z coordinates of the nth monomer and the polymer center of mass, respectively. The brackets $\langle \ldots \rangle$ denote an average over the conformations sampled at all times in the cycle of the flashing ratchet. The quantity $\langle R_z^2 \rangle_{\text{eq}}$ is defined similarly to $\langle R_z^2 \rangle$, except for a free polymer in equilibrium, i.e., in the *absence* of the flashing ratchet. Note that $\langle R_z^2 \rangle_{\text{eq}} = R_{\text{g}}^2/3$, where the equilibrium radius of gyration of the polymer, R_{g}, is given by

$$R_{\text{g}}^2 = \sum_{n=1}^{N} \langle (\vec{r}_n - \vec{r}_{\text{cm}})^2 \rangle_{\text{eq}}, \tag{15}$$

where $\vec{r}_n$ is the position of monomer n and $\vec{r}_{\text{cm}}$ is the polymer center of mass.

Figure 3(a) shows the measured β_z vs L for several polymer lengths for the HD system. These data were generated from the same simulations corresponding to the data in Fig. 2(b). Note that in most cases $\beta_z < 1$, indicating that the flashing ratchet induces a compression of the polymer along the ratchet axis. The degree of compression depends on the polymer length and the ratchet spatial period. The variation in β_z with L is qualitatively similar for each N. Specifically, β_z has a single minimum located at a ratchet length that we label L_β^*. For $L > L_\beta^*$, β_z increases slowly with L, while for $L < L_\beta^*$, β_z rises rapidly with decreasing L. Comparison of Figs. 2(b) and 3(a) reveals that the value of L_β^* for each N corresponds closely to the location of the convergence points for v_z that were described in the previous section. The exact same pattern holds for the non-HD results (data not shown). Assuming that the earlier interpretation of Fig. 2 is correct, $L \gtrsim L_\beta^*$ corresponds to the regime where center-of-mass diffusion is a significant part of the mechanism for polymer transport, and $L \lesssim L_\beta^*$ corresponds to the regime where it is not. Thus, there is appears to be a quantitative correlation between the mode of transport of the polymer and its average conformational state, independent of whether HD interactions are present or not.

The trends in Fig. 3(a) can be better understood by inspection of Fig. 3(b), which shows β_z vs $\alpha L/R_g$ for the same data. Recall that the distance αL is the distance from potential minimum to the nearest maximum (see Fig. 1) and is the key ratchet length scale that determines when a diffusive

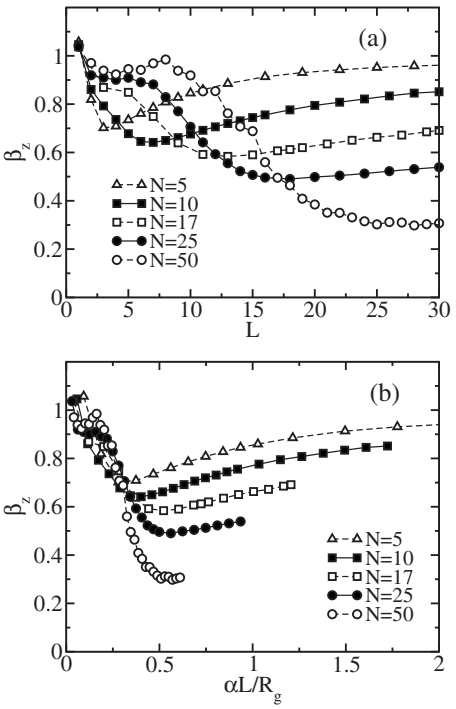

FIG. 3. (a) Polymer deformation factor, β_z, vs ratchet spatial period, L, for several N. For these data, HD interactions are present in the simulation model. Note that $t_{\text{off}} = t_{\text{on}} = 20$, $V = 4$, and $\alpha = 0.1$. (b) The same data as in (a), except plotted vs $\alpha L/R_g$.

particle in the flashing ratchet will undergo a stepping event when the potential is turned back on. If $\alpha L/R_g$ is sufficiently large, the polymer will likely span a single ratchet spatial period between two adjacent maxima. In this regime, β_z should increase as L increases, as this corresponds to an effective widening of the potential well; this trend is evident in both Figs. 3(a) and 3(b). Intuitively, one also expects that if the ratio $\alpha L/R_g$ is sufficiently small, the polymer will be increasingly likely to span multiple periods of the ratchet, even when the potential is in the on-state. The consequence will be a reduction in the average compression (or even an expansion) of the polymer and, thus, an increase in β_z with decreasing L for sufficiently low L. Figure 3(b) shows that the minima for β_z, which mark the onset of the regime where the polymer spans multiple potential wells, occur for comparable values of this ratio of length scales, i.e., $\alpha L/R_g \approx 0.3-0.5$. It is possible that the shift in the location of the minima for $N=5$ and 10 is a finite-size effect and that the $\alpha L_\beta^*/R_{\text{g}}$ converges to a fixed value as N increases. However, the present data are insufficient to determine the precise relationship between αL_β^* and R_{g} for long chains. Results for the non-HD system are quantitatively consistent with these trends. In that case, αL_β^* are slightly lower for each N (data not shown).

The deformation factor β_z defined in Eq. (13) involves averaging over conformations at all times during the ratchet cycle. Note, however, that the degree of deformation undergoes a cyclic compression and relaxation behavior as the ratchet is toggled on and off, respectively. The rates of these processes are expected to be affected by the polymer length and HD interactions. In addition, the degree of compression

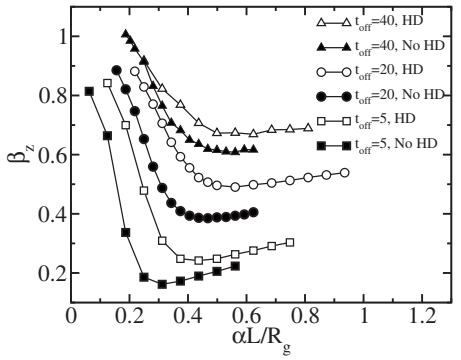

FIG. 4. Polymer deformation factor, β_z, vs $\alpha L/R_g$, for polymer length $N=25$. Results are shown for three different values of t_{off}, in each case with and without HD interactions. Note that $t_{on}=20$, $V=4$, and $\alpha=0.1$.

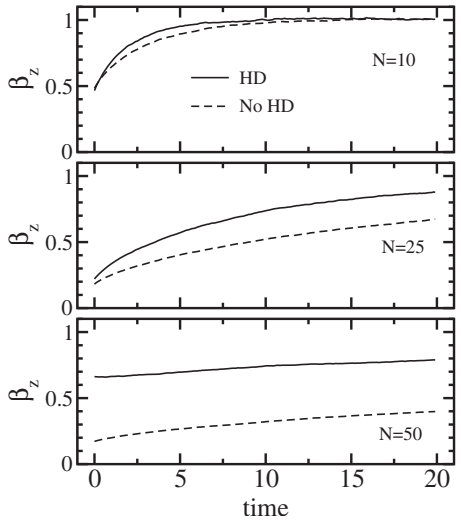

FIG. 5. Time-dependent deformation factor, β_z, vs time during the off-phase of the ratchet cycle for $t_{off}=20$. Results are shown for three different chain lengths, each for HD and non-HD systems. For each case, $L=14$, $t_{on}=20$, $V_0=4$, and $\alpha=0.1$.

and relaxation achieved over each cycle clearly depends on the times t_{on} and t_{off}. Consequently, the values of these cycle times should affect both β_z and the transport behavior of the polymer in the Brownian ratchet.

Let us consider the effect of t_{off} on the behavior of the system. Figure 4 shows β_z vs $\alpha L/R_g$ for $N=25$ for $t_{off}=5$, 20, and 40. In each case, results for both the HD and non-HD systems are shown. Variation of this ratchet cycle time constant has two notable effects on the conformational behavior of the polymer. First, β_z decreases when t_{off} decreases. This arises because the ratchet is on a larger fraction of the cycle time when t_{off} is decreased while t_{on} is held fixed. A more significant trend is the fact that L_β^* increases as t_{off} increases. The origin of this behavior relates to the conformational relaxation that occurs during the off-phase of the cycle. We propose the following explanation. Consider a polymer of length N in a ratchet of length L. If the polymer is confined to the vicinity of a single ratchet potential minimum during the on-phase, it will relax from a highly flattened shape toward its equilibrium spherical shape during the off-phase. This process will be characterized by a relaxation time, τ_r. If $t_{off} \ll \tau_r$, then the polymer will remain flattened and will likely be captured by a single ratchet minimum during the next on-phase of the cycle. Thus, it is likely to be in the $L < L_\beta^*$ regime. As t_{off}/τ_r increases, an initially flattened polymer will have sufficient time to broaden along the z direction, increasing the likelihood that it will span multiple minima when the ratchet is turned back on, and, thus, that the polymer will be in the $L > L_\beta^*$ regime. As t_{off}/τ_r further increases, it will cross into a regime where the polymer is fully relaxed, and thus a further increase in t_{off} will lead to no further effect. The predicted trend then is that L_β^* increases with t_{off} for $t_{off} \lesssim \tau_r$ and that L_β^* is independent of t_{off} for $t_{off} \gg \tau_r$. In addition, L_β^* should increase as τ_r decreases.

To test the applicability of this explanation, we obtained the relaxation time, τ_r, from an analysis of the time correlation function of R_z^2 for a free polymer. In the large-t regime, the correlation function crosses over into an exponential decay corresponding to the relaxation of the slowest internal mode, and τ_r was taken to be the corresponding time constant. For $N=25$, we measure $\tau_r=10.5$ with HD and $\tau_r=27.9$ without HD. In the HD case, $\tau_{off}=5$, 20, and 40 corresponds to $\tau_{off}/\tau_r=0.48$, 1.9, and 3.8. We note that there is a significant shift in L_β^* between the cases of $\tau_{off}=5$ and 20, which span a range of times over which the polymer shape is still relaxing. On the other hand, there is little change in L_β^* in changing t_{off} from 20 to 40, which span a range of times over which the polymer shape will not have relaxed appreciably further. For the non-HD polymer, $t_{off}=5$, 20, and 40 corresponds to $t_{off}/\tau_r=0.18$, 0.72, and 1.43. The degree of relaxation differs appreciably for each of these t_{off} times, which correlates well with the consistent increase in L_β^* with t_{off} evident in the figure.

The impact of HD interactions on β_z for any given value of t_{off} is also consistent with this interpretation. The fact that τ_r is appreciably lower in the HD case than in the non-HD case is consistent with the fact that L_β^* is generally higher in the latter case. Moreover, this difference in L_β^* for the two cases is expected to diminish where t_{off} is sufficiently large that both HD and non-HD polymers have relaxed. As observed in the figure, the minima of β_z for $t_{off}=40$ occur at approximately the same L_β^*, consistent with the fact that t_{off}/τ_r in each case is sufficiently large that the polymer will be mostly relaxed.

Let us now investigate the details of the conformational relaxation during the off-phase of the ratchet cycle. To do this, we introduce a time-dependent deformation factor, $\beta_z(t)$, which is defined the same as in Eqs. (13) and (14), except that conformational averaging of $\langle R_z^2 \rangle$ is performed at specific times in the ratchet cycle. Here, $t=0$ is defined to be the time when the ratchet potential is turned off. Figure 5 shows $\beta_z(t)$ vs time for polymers of length $N=10$, 25, and 50 calculated for a ratchet of length $L=14$ during the off-phase of the cycle, with $t_{off}=20$. In each case, results HD and non-HD systems are shown. There are two key trends: (1) the relaxation rate decreases with increasing chain size, and (2) the relaxation is faster when HD interactions are included.

These trends can be understood by a comparison with the dynamical behavior of a free polymer in equilibrium. Recall

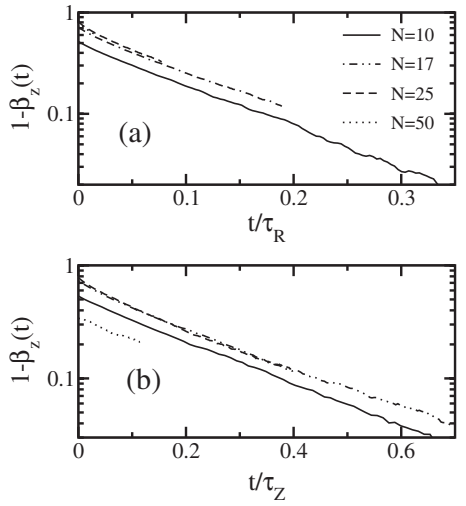

FIG. 6. (a) Time dependence of the deformation factor for the non-HD, shown as $1-\beta_z(t)$ vs t/τ_R, where $\tau_R=R_g^2/D$ is the Rouse time of the polymer. Results are shown for three different polymer lengths. (b) As in (a), except for the HD system, and where the time is scaled by $\tau_Z=R_g^2/D$, the Zimm time of the polymer.

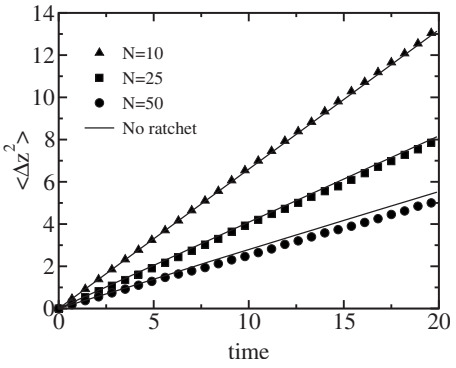

FIG. 7. Mean-squared displacement along the z direction of the polymer center of mass vs time. Simulation results are shown for three different chain lengths. HD interactions are present. The solid symbols are data for the polymer in a flashing ratchet during the *off-phase* of the ratchet cycle, while the solid curves show corresponding results for a polymer in the absence of a flashing ratchet (i.e., a free polymer). For the polymer/ratchet simulations, $L=18$ and $t_{on}=t_{off}=20$.

that the Rouse and Zimm times, τ_R and τ_Z, respectively, are defined

$$\tau_R = R_g^2/D_R, \tag{16}$$

$$\tau_Z = R_g^2/D_Z, \tag{17}$$

where D_R and D_Z are the diffusion coefficients for the Rouse (non-HD) and Zimm (HD) cases, respectively. These are the times over which a polymer will diffuse a distance equal to its equilibrium radius of gyration, R_g. Note that the each of these times obeys the same scaling relation as that of the slowest internal mode of motion of the polymer; that is, $\tau_R \propto N^{1+2\nu} \approx N^{2.2}$ (non-HD) and $\tau_Z \propto N^{3\nu} \approx N^{1.8}$ (HD) [48]. Figure 6 shows plots of the time-dependence $1-\beta_z$ using the data from Fig. 5, with the time variable scaled by τ_R for the Rouse case and τ_Z for the Zimm case, each of which was obtained from simulations of a free polymer for the model employed. Over the time period considered, $1-\beta_z(t)$ relaxes approximately exponentially; that is,

$$1-\beta_z \propto \begin{cases} \exp[-t/(a_R\tau_R)], & \text{(Rouse)} \\ \exp[-t/(a_Z\tau_Z)], & \text{(Zimm)} \end{cases} \tag{18}$$

where the two constants are approximately $a_R \approx 0.1$ and $a_Z \approx 0.2$. In each case, the values of decay constants, $a_R\tau_R$ and $a_Z\tau_Z$ are consistent with the equilibrium relaxation times obtained from an analysis of the time correlation function of R_z^2, which was described earlier.

Let us review the main conclusions in this section and discuss their significance. The key point is that the mode of transport of the polymer in the Brownian ratchet is correlated with the polymer's conformational behavior. In the low-N/high-L regime, the compression factor β_z increases slightly with increasing L. We propose that this regime corresponds to a mode of transport for which polymer center-of-mass diffusion is significant; this is reflected by the fact that $\langle v_z \rangle$ is sensitive to changes in N in this regime. By contrast in the high-N/low-L regime, the average polymer compression increases with *decreasing* L. This appears to correspond to a regime in which center-of-mass diffusion is not an integral part of the transport mode; this is reflected by the fact that $\langle v_z \rangle$ is independent of polymer length. The regime crossover point occurs in the vicinity of L_β^*, the location of the minimum in the β_z vs L curves. The results in this section facilitate identification of the regime using equilibrium polymer properties such as R_g and τ_Z (or τ_R for systems where HD interactions are screened) and the Brownian ratchet parameters such as L and t_{off}.

C. Effects of deformation on diffusion during the off-phase

During the off-phase of the ratchet cycle, the polymer undergoes free diffusion with equal probability of moving forward or backward along the ratchet axis. The rate of diffusion during this phase strongly affects the velocity of a particle driven by flashing ratchet. For the polymer/ratchet system here, we expect this to be true for the low-N/high-L regime described above. As noted in a recent study, [9] however, the shape deformations described in Sec. III B can affect the rate of diffusion and, consequently, $\langle v_z \rangle$.

To investigate this effect for the present model system we have calculated $\langle (\Delta z)^2 \rangle$, the mean-square displacement of the polymer center of mass along the z direction during the off-phase. Results are shown in Fig. 7 for $N=10$, 25, and 50 for the HD model system for $L=18$. For a free polymer (i.e., no ratchet potential) this quantity satisfies

$$\langle (\Delta z)^2 \rangle = 2Dt, \tag{19}$$

where D is the diffusion coefficient of the free polymer. Displacement curves calculated using Eq. (19) for the same three polymer lengths are also shown in the figure. For $N=10$, the results for the polymer/ratchet system and those calculated using Eq. (19) are quantitatively consistent. However, for $N=25$ the polymer diffuses more slowly during the

off-phase of the ratchet cycle relative to the free polymer. This difference is even larger for $N=50$.

This effect was first observed in the recent study by Kenward and Slater, [9] whose explanation can be summarized as follows. When HD interactions are present, and the diffusional behavior of the polymer is essentially that of as a solid object with dimensions comparable to the average dimensions of the polymer. Thus, a free polymer diffuses like a sphere with a radius comparable to R_g. The flashing ratchet compresses the polymer into a highly oblate shape that is flattened along z, which then slowly relaxes back to equilibrium during the off-phase of the cycle. This shape anisotropy affects the rate of diffusion. A polymer flattened along z diffuses more slowly in this direction than one in a spherical shaped conformation. The relaxation of the shape anisotropy leads to a time-dependent diffusion coefficient, which is initially slower for the oblate shape and which gradually increases as the polymer becomes more spherical. For short polymers, the conformational relaxation is sufficiently rapid that the effect of an initially slower rate of diffusion is negligible. For longer polymers, the shape anisotropy is appreciable during the entire off-phase and the rate of diffusion is slower. In the absence of hydrodynamics, the rate of diffusion is unaffected by the conformation behavior of the polymer. Consequently, the time-dependence of $\langle(\Delta z)^2\rangle$ during the off-phase of the ratchet cycle is the same as that for a free polymer. This was confirmed by our simulation results (data not shown).

D. Localization during the on-phase

The flashing ratchet mechanism requires that the probability distribution of the transported particle be asymmetric with respect to the midpoint between successive maxima at the end of the on-phase of the cycle. Effective and coherent transport is best achieved when V_0/k_BT is sufficiently large that the transported particle become localized near a potential well during this phase. The nature and degree of localization for highly flexible polymer chains depends strongly on properties such as polymer length, as well as the values of ratchet parameters such as t_{on}, t_{off}, V_0, and α. In the present study, we have not carried out an extensive investigation of localization over this parameter space but instead have focused on a narrower parameter regime for the purpose of elucidating the transport behavior described in Sec. III A.

Figure 8 shows $\mathcal{P}_{on}(z_{cm}/L)$, the center-of-mass position probability distributions (scaled by the ratchet spatial period) calculated at the end of the on-phase of the ratchet cycle, for the $N=10$ polymer for a range of L corresponding to the low-N/high-L regime described earlier. Several trends are apparent. First, the center of mass is localized over a small range of positions shifted to the left of the ratchet minimum at $z_{cm}/L=0.9$. The degree of the shift away from the minimum monotonically increases as L decreases. In addition, the unscaled distributions shown in the inset reveal that degree of localization (quantified by the height or reciprocal of the width of the probability peak) increases as L decreases. Comparison with the $N=10$ curve of Fig. 3(a) shows that the degree of polymer localization is positively correlated with

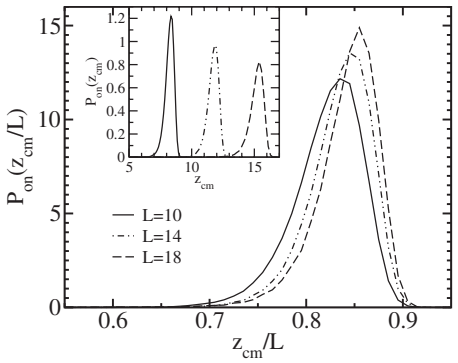

FIG. 8. Probability distribution of the polymer center of mass, $\mathcal{P}_{on}(z_{cm}/L)$ vs scaled center-of-mass position, z_{cm}/L. The ratchet potential minimum is located at $z_{cm}/L=0.9$, and the maxima are located at $z_{cm}/L=0$ and $z_{cm}/L=1$. The distributions are calculated at the end of the on-phase of the ratchet cycle. Data are shown for a polymer of length $N=10$ in the presence of HD interactions for $L=10$, 14, and 18. The inset shows the unscaled versions of the same probability distributions.

the degree of polymer compression induced by the ratchet. These results are comparable with those reported in Ref. [9] for a similar model system. Note that the polymer will become more effectively localized at the ratchet minimum as V_0/k_BT increases.

Figure 9 shows the distribution of the center of mass of a $N=50$ polymer for $L=6$, 10, and 14. Inspection of the $N=50$ curve of Fig. 3 shows that this corresponds to the high-N/low-L regime, where center-of-mass diffusion does not appear to be the dominant transport mechanism. As in the case shown in Fig. 8, the distribution peaks at a position that is shifted to the left of the potential minimum ($z_{cm}/L=0.9$) by an amount that increases with decreasing L. For the same values of L, the peak widths are narrower than those for $N=10$, though the peak positions are approximately the same. This trend is consistent for other chain lengths as well (data not shown). The most notable feature in the data, however, is

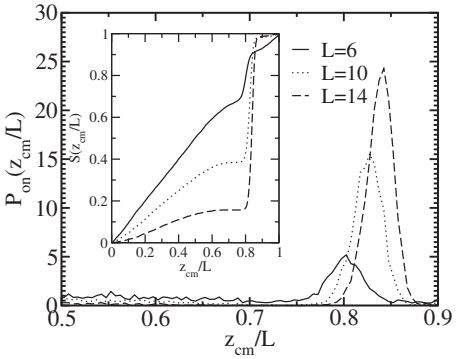

FIG. 9. Probability distribution of the polymer center of mass, $\mathcal{P}_{on}(z_{cm}/L)$ vs scaled position, z_{cm}/L. The ratchet potential minimum is located at $z_{cm}/L=0.9$, and the maxima are located at $z_{cm}/L=0$ and $z_{cm}/L=1$. The distributions are calculated at the end of the on-phase of the ratchet cycle. Data are shown for a polymer of length $N=50$ in the presence of HD interactions for $L=6$, 10, 14, and 18. The inset show the running integral $S(z_{cm}/L)=\int_0^{z_{cm}/L} d(z'_{cm}/L)\mathcal{P}_{on}(z'_{cm}/L)$.

the appreciable probability that the polymer center of mass lies outside the range covered by the dominant peak. The relative importance of this second component of the distribution is evident by the inset of the figure, which shows the running integral of the distribution, $S(z_{cm}/L) = \int_0^{z_{cm}/L} d(z'_{cm}/L)\mathcal{P}(z'_{cm}/L)$, for each data set. Clearly, as L decreases, the probability that z_{cm} lies outside the narrow range defined by the peak *increases*. The origin of this trend is straightforward. As L decreases, there is an increasing likelihood that the polymer will span at least two successive potential minima at the end of the on-phase. In such cases, the polymer center-of-mass position is increasingly likely to be located further from any single minimum. Thus, the intensity of the main peak decreases and the intensity of the broad component of the distribution increases as L is decreased. This result supports our interpretation of the data in Figs. 2 and 3 with regard to the physical meaning of the high-N/low-L regime.

Finally, the probability distributions in the low-N/high-L regime were not measurably different in the HD and non-HD cases for the parameter values relevant for the data in Figs. 2 and 3. As the dynamical response of the HD polymer to the application of the external potential is expected to be more rapid than that of the non-HD polymer, we infer that $P_{on}(z_{cm})$ has reached its equilibrium value by the end of the on-period ($t_{on}=20$) in those simulations. This was confirmed, in part, by the results of additional simulations carried out for $t_{on} > 20$. For some range of t_{on} below $t_{on}=20$, $P_{on}(z_{cm})$ is expected to differ between the HD and non-HD cases. Further simulation work is required for a more complete understanding of localization, but is outside the scope of the present study.

E. Theoretical description of polymer transport in the low-N or high-L regime

In their experimental studies of the transport behavior of DNA fragments in a micromachined Brownian ratchet device, Bader *et al.* employed a simple theoretical model to interpret the data. [4–6] The model treats the fragments as structureless particles acting in the same one-dimensional flashing ratchet potential employed here [49]. In the experimental system, $R_g \ll \alpha L$, which corresponds to the low-N/high-L regime described above. To gain deeper insight into the mechanism driving the polymer motion and to better understand the role of HD interactions in this experimentally relevant regime, we review the theory and apply it to our simulation results.

The theoretical model first assumes that t_{on} and the ratchet barrier height V_0 are both sufficiently large that the particle will be localized at a potential minimum, z_{min}, at the end of the on-phase of the ratchet cycle. During the off-phase of the cycle, the particle freely diffuses, and at the end of this phase the particle position probability distribution, $\mathcal{P}_{off}(z)$, is given by

$$\mathcal{P}_{off}(z) = \frac{\exp[-(\Delta z)^2/4Dt_{off}]}{\sqrt{4\pi D t_{off}}}, \tag{20}$$

where $\Delta z = z - z_{min}$ and z is the coordinate of the particle. Transport is achieved in the case when t_{off} is sufficiently long for the particles to diffuse easily to the right (with reference to Fig. 1) over the short distance (αL) from the minimum to a maximum, but sufficiently short to avoid appreciable back-diffusion over a distance $(1-\alpha)L$. All particles which have advanced to the right by αL will be driven by the ratchet to the next minimum by the end of the next on-phase of the ratchet cycle. In this approximation, it is easy to show that the probability, s, of the particles advancing one period, L, to the right over one temporal period is

$$s = \frac{1}{2}\mathrm{erfc}(\alpha L/\sqrt{4Dt_{off}}) \tag{21}$$

and the average velocity is given by

$$\langle v_z \rangle = sL/\tau, \tag{22}$$

where $\tau \equiv t_{on} + t_{off}$ is the temporal period of the ratchet.

The application of this simple theory to a polymer is clearly problematic. The distribution of many interaction sites (i.e., monomers) along the transport axis means that the magnitude and direction of the net force on the polymer at any one time does not have the same trivial dependence on position as in the case of a single particle. Consequently, the dynamical behavior is expected to be different. A striking example of such behavior was noted in a recent study of 1D systems of rigid rodlike dimers and trimers in a flashing ratchet motor [24], wherein it was observed that the velocity can reverse direction multiple times in response to changing the length of the chain or system temperature. In addition, the flexibility of the polymer introduces the further complication that the polymer conformation will respond to the ratchet potential, with corresponding effects on the rate of transport [8,9]. Nevertheless, the theory should at least become valid in the limit where the size of the polymer is sufficiently small relative to αL.

To apply this simple theory to a diffusive polymer, we first define the polymer position as the location of the center of mass, z_{cm}. Next, we note that the diffusion coefficient for an *undeformed* polymer chain scales with N as

$$D = \frac{k_B T}{\gamma} = \frac{kT}{C\gamma_0 N^{\delta}}, \tag{23}$$

where γ and γ_0 is the friction coefficient for the polymer and for a single monomer, respectively. In the absence of HD interactions, $C=1$ and $\delta=1$. In the presence of HD interactions $\delta=\frac{3}{5}$ and the constant C depends on the details of the molecular model. Measurement of the time dependence of the polymer center-of-mass mean-square displacement was used to calculate the diffusion coefficient for several different chain lengths. This yielded a value of $C \approx 0.70$ for the longer polymer chains, with small deviations for shorter chains attributable to finite-size effects. The value of L that maximizes the velocity is calculated using Eqs. (21) and (22), and the condition that $d\langle v_z \rangle / dL = 0$. Numerical solution of the resulting nonlinear equation yields $\alpha L/\sqrt{4Dt_{off}} = 0.5316$. Using this result together with Eq. (23), the theory predicts a maximum velocity at a spatial period L^* given by

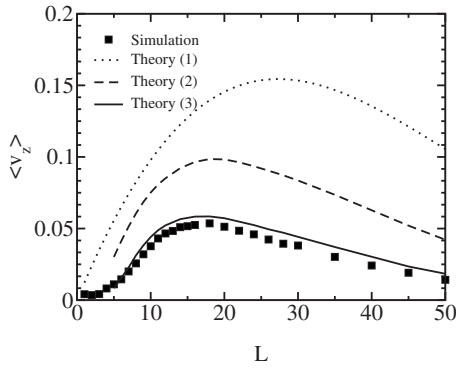

FIG. 10. Polymer center-of-mass velocity $\langle v_z \rangle$ vs L for a polymer of length $N=10$ in the presence of HD interactions. In addition to the simulation results, the figure shows three sets of theoretical predictions: (1) using Eqs. (21)–(23); (2) using Eqs. (22) and (23) together with Eq. (28) and probability distributions $\mathcal{P}_{\rm on}(z_{\rm cm})$ measured from the simulation; and (3) using Eqs. (29)–(33), as well as the probability distribution $\mathcal{P}_{\rm on}(z_{\rm cm})$ and the quantity $\bar{R}_z$, each of which was taken from the simulation results.

$$L^* \approx \frac{1.063}{\alpha}\sqrt{\frac{k_B T t_{\rm off}}{\gamma_0}}\frac{N^{-\delta/2}}{\sqrt{C}}. \tag{24}$$

From Eqs. (21) and (22), the maximum value of the velocity, $v_{\rm max}$ is given by $v_{\rm max}=L^*{\rm erfc}(0.5316)/(2\tau)$, which reduces to

$$v_{\rm max} = \frac{0.2404}{\alpha\tau}\sqrt{\frac{k_B T t_{\rm off}}{\gamma_0}}\frac{N^{-\delta/2}}{\sqrt{C}}. \tag{25}$$

Thus, the theory predicts that $v_{\rm max}$ and L^* both *decrease* with increasing chain length N independent of whether HD interactions are present or absent. As noted earlier, this trend is observed in both sets of simulation results of Fig. 2 in the regime of small N, i.e., in the regime where the theory is expected to be valid. In addition, the theory predicts that L^* and $v_{\rm max}$ should both be *greater* when HD interactions are present, which is at least consistent with the observed trends in the low-N/high-L regime. However, while the theory is qualitatively correct in this regime, the quantitative predictions are consistently poor. Figure 10 shows the prediction [labeled "Theory (1)"] for a $N=10$ polymer with HD interactions using Eqs. (21)–(23) overlaid on the simulation data. The theoretical model predicts $\langle v_z \rangle$ to be much larger than the true value. In addition, the location of the maximum, L^*, is too large by roughly a factor of two. These quantitative discrepancies are present for all other polymer lengths studied, independent of whether HD interactions are included.

The inconsistency between the theoretical predictions and the simulation data for the short chains imply that at least one of the approximations employed in the theory is not valid. The key approximations are the following: (1) the polymer center of mass is located at a ratchet potential minimum at the end of the on-phase of the ratchet cycle; (2) the polymer center-of-mass probability distribution function at the end of the off-phase is given by Eq. (20), where D is the diffusion coefficient of a *free* polymer; (3) the polymer is advanced to the next potential minimum after the potential is turned back on if its center of mass has diffused past the position of the nearest potential maximum during the off-phase [this condition is implicit in Eqs. (21) and (22)].

As discussed in Sec. III D, the polymer system in the present study clearly does *not* satisfy condition (1), at least for the parameter range used here. Rather the polymer average position is consistently displaced to the shallow side of the asymmetric potential well (see Fig. 8). This is expected to be a better approximation for any given N and L, however, as V_0 increases. As discussed in Sec. III C, condition (2) is true for the HD system for sufficiently short polymer length. However, as for greater N, the ratchet-induced shape deformation effectively reduces the rate of diffusion relative to that predicted using the value of D for an undeformed polymer.

In order to test the validity of condition (3), we modify Eq. (21) by removing the first two approximations from the calculation. To bypass condition (1), we can integrate over the $P_{\rm on}(z_{\rm cm})$ distributions measured from the simulations (such as those shown in Fig. 8). Next, we note that the characteristic distance, $l_{\rm D}$ traversed by a diffusive particle over a time $t_{\rm off}$ is

$$l_{\rm D} \approx \sqrt{2Dt_{\rm off}}. \tag{26}$$

To circumvent condition (2), we use instead

$$l_{\rm D} = \sqrt{\langle \Delta z^2(t_{\rm off})\rangle}, \tag{27}$$

where the right-hand side of the equation is the root-mean-square distance traveled by the particle along the ratchet axis during the off-phase in the simulation. Consequently, we have

$$s = \int_0^L dz P_{\rm on}(z_{\rm cm}){\rm erfc}[(L-z_{\rm cm})/\sqrt{2}l_{\rm D}], \tag{28}$$

where $l_{\rm D}$ is evaluated using Eq. (27). Figure 10 shows a comparison of the predicted values of $\langle v_z \rangle$ using the different theoretical models and the values obtained from simulation [labeled "Theory (2)"]. As expected, using Eq. (28) significantly improves the accuracy of the theoretical predictions in the non-HD and HD cases. However, the values of the predicted $\langle v_z \rangle$ from the revised theory are still rather poor. The velocities are approximately two times greater than the simulation values, and the situation is even worse for the non-HD case. Consequently, we conclude that approximation (3) is not valid. The overestimate of $\langle v_z \rangle$ suggest that there is a significant probability that polymers whose centers of mass have diffused past the location of a ratchet potential maximum are *not* advanced to the next minimum when the potential is turned back on. The origin of this effect is rooted in the asymmetry of the potential around the local maxima. Consider a short polymer whose center of mass has diffused just past the position of the nearest maximum when the potential is turned back on. If the distribution of monomers is symmetrically distributed close to the center of mass, then approximately half the monomers will be located to the left of the maximum and each will experience a force $F_z = -V_0/(\alpha L)$, while the other half of the monomers will be located to the right of the maximum and will feel a consid-

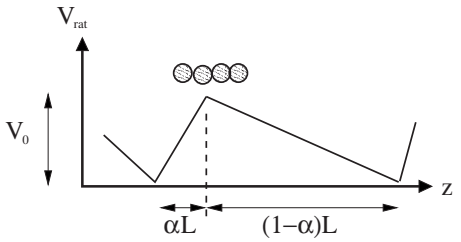

FIG. 11. Illustration showing why a polymer could fail to be driven to the next ratchet minimum even when its center of mass has diffused past the location of the nearest ratchet maximum. The two monomers to the left of the maximum are each pushed to the left with a force of magnitude $F=V_0/(\alpha L)$, while the two monomers to the right of the maximum are pushed to the right with a *smaller* force of magnitude $F=V_0/((1-\alpha)L)$. Thus, the polymer will tend to be driven back to the left.

erably weaker force, $F_z=-V_0/[(1-\alpha)L]$. Thus, when the potential is turned on, the instantaneous force will act to drive the polymer back to its original potential minimum. This effect is illustrated in Fig. 11 for a short polymer. Only when the polymer center of mass has diffused sufficiently far past the potential maximum will the net instantaneous force become positive and thus drive the polymer to the next minimum. Of course, this simple picture neglects complicating effects such as the distortion of the polymer shape by the ratchet potential and the subsequent effects on the dynamics. However, it is expected to be relevant for sufficiently short polymers and large L.

Let us consider a simple alternative criterion for determining when a polymer advances to the next potential minimum when the ratchet potential is turned on. Such a condition clearly must involve the distribution of monomer positions along the z axis. A measure of the width of this distribution is the quantity $\bar{R}_z$, which is defined

$$\bar{R}_z^2 \equiv \langle R_z^2 \rangle_{\text{off}}, \tag{29}$$

where the instantaneous value of R_z was defined in Eq. (14), and the angular brackets $\langle \ldots \rangle_{\text{off}}$ in Eq. (29) denote an average over conformations sampled at the end of the off-phase of the ratchet cycle. In the limit where t_{off} is large compared to the longest conformational relaxation time of the polymer, $\bar{R}_z=R_g/\sqrt{3}$, where R_g is the equilibrium root mean square radius of gyration of the polymer in the absence of any external potential. Let us assume the monomer position distribution function is a Gaussian distribution:

$$\mathcal{P}_{\text{mon}}(z;z_{\text{cm}},\bar{R}_z) = \frac{1}{\sqrt{2\pi\bar{R}_z^2}} \exp\left[-\frac{(z-z_{\text{cm}})^2}{2\bar{R}_z^2}\right]. \tag{30}$$

If the ratchet force on a single monomer is $f_z=f_z(z)$, then the average net force on the polymer generated by the ratchet is given by

$$\bar{F}_z(z_{\text{cm}},\bar{R}_z) = N\int_{-\infty}^{\infty} dz f_z(z)\mathcal{P}_{\text{mon}}(z;z_{\text{cm}},\bar{R}_z). \tag{31}$$

To a first approximation, we expect that the polymer will advance to the next potential minimum if its center of mass has advanced to the right of the nearest maximum and $F_z>0$. The probability, s, of the polymer advancing to the next potential minimum is obtained by the following integration:

$$s = \int_{-\infty}^{\infty} dz_{\text{cm}} \mathcal{P}_{\text{off}}(z_{\text{cm}}) \mathcal{S}(R_{g,z}^2, z_{\text{cm}}), \tag{32}$$

where

$$\mathcal{S}(\bar{R}_z, z_{\text{cm}}) = \begin{cases} 1, & F_z(\bar{R}_z, z_{\text{cm}}) > 0 \\ 0, & F_z(\bar{R}_z, z_{\text{cm}}) < 0 \end{cases}$$

and where $\mathcal{P}_{\text{off}}(z_{\text{cm}})$ is the polymer center-of-mass probability distribution at the end of the off-phase of the cycle and is given by

$$\mathcal{P}_{\text{off}}(z_{\text{cm}}) = \frac{1}{\sqrt{2\pi}l_{\text{D}}} \int_0^L dz'_{\text{cm}} \mathcal{P}_{\text{on}}(z'_{\text{cm}}) \exp\left[-\frac{(z_{\text{cm}}-z'_{\text{cm}})^2}{2l_{\text{D}}^2}\right], \tag{33}$$

where $P_{\text{on}}(z_{\text{cm}})$ is the center-of-mass distribution function at the end of the on-phase of the cycle, as defined earlier. The distance l_{D} can be taken from simulations using Eq. (26). In practice, though, the approximation of Eq. (27) was sufficient for most cases here. Equation (32) can then be used with Eq. (22) to predict $\langle v_z \rangle$. This requires knowledge of the distribution $\mathcal{P}_{\text{on}}(z_{\text{cm}})$ and the quantity $\langle R_z^2 \rangle$, each of which is obtained from the simulations. Examples of $\mathcal{P}_{\text{on}}(z_{\text{cm}})$ for different L were shown in Fig. 8. The theoretical predictions of $\langle v_z \rangle$ using Eqs. (29)–(33) are shown in Fig. 10 [labeled "Theory (3)"]. Clearly, this refined version of the theory that corrects the problems of the approximations of the original theory leads to significantly better prediction of $\langle v_z \rangle$, whether or not HD interactions are present.

Figures 12(a) and 12(b) show the theoretical predictions using Eqs. (29)–(33) of $\langle v_z \rangle$ for $N=5$ and $N=10$, respectively, overlaid on the simulation data. Results for both HD and non-HD systems are shown, and for $t_{\text{off}}=10$ and 20. The data are shown for the scaled velocity, $\langle v_z \rangle \tau/L$, vs the scaled ratchet spatial period, $\alpha L/\sqrt{2Dt_{\text{off}}}$, where D is the diffusion coefficient for the free polymer in equilibrium (i.e., no ratchet). The inset of each figure shows the same data in unscaled form, i.e., $\langle v_z \rangle$ vs L. Note that the scaled independent variable, $\alpha L/\sqrt{2Dt_{\text{off}}}$, is a ratio of two length scales: αL is the key length scale of the ratchet potential that determines the velocity of a particle in the flashing ratchet, and $\sqrt{2Dt_{\text{off}}}=l_{\text{D}}$ is characteristic distance traveled by the particle during the off-phase of the cycle (ignoring the effects of polymer deformation on D). In the context of the original theory [49] used by Bader *et al.* to interpret their experimental data [4–6] [i.e., Eqs. (21) and (22)] the data should all fall on a universal curve, regardless of the value of t_{off} or whether HD interactions are present or absent. For $N=5$, the simulation data collapse is reasonably good, in spite of the

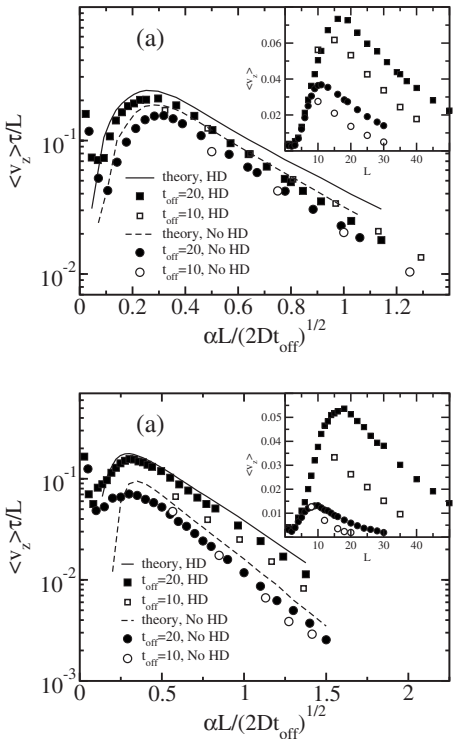

FIG. 12. (a) Scaled polymer center-of-mass velocity $\langle v_z \rangle \tau / L$ vs scaled ratchet length $\alpha L / \sqrt{2Dt_{\mathrm{off}}}$ for a $N=5$ polymer. Results for two different t_{off} values are shown for both HD and non-HD systems. The solid and dashed lines show the theoretical predictions using Eqs. (22) and (29)–(33) for $t_{\mathrm{off}}=20$. The inset shows the same data plotted as $\langle v_z \rangle$ vs L. (b) As in (a), except for $N=10$.

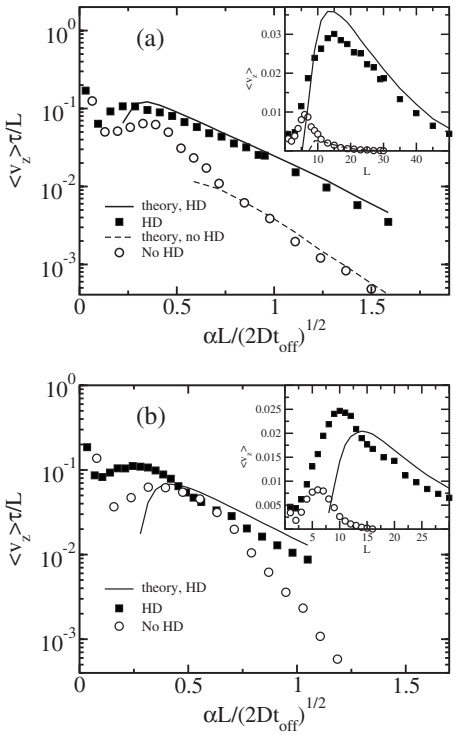

FIG. 13. (a) Scaled Polymer center-of-mass velocity $\langle v_z \rangle \tau / L$ vs scaled ratchet length $\alpha L / \sqrt{2Dt_{\mathrm{off}}}$ for a $N=17$ polymer. Results shown for both HD and non-HD systems for $t_{\mathrm{off}}=20$. The solid and dashed lines show the theoretical predictions using Eqs. (22) and (29)–(33) for $t_{\mathrm{off}}=20$. The inset shows the same data plotted as $\langle v_z \rangle$ vs L. (b) As in (a), except for $N=25$. Only the theoretical prediction for the HD system is shown.

wide spread between the unscaled data curves shown in the inset. The graphs also show the theoretical predictions using Eqs. (22) and (29)–(33) for the $t_{\mathrm{off}}=20$ data. The predictions are reasonably good although the theory does consistently overestimate $\langle v_z \rangle$ slightly for both the HD and non-HD cases. The predictions only begin to diverge significantly from the data at very low L. This feature is consistent with the interpretation of the results in Figs. 2 and 3 described in Secs. III A and III B, i.e., the data correspond to the low-N/high-L regime for $L \gtrsim 5$ for $N=5$ with $t_{\mathrm{off}}=20$. The theoretical predictions for $\langle v_z \rangle$ for $N=10$ shown in Fig. 12(b) are also in reasonable agreement with the simulation data; again, however, the theory does slightly overestimate the values. At values of $\alpha L / \sqrt{2Dt_{\mathrm{off}}}$ corresponding approximately to the high-N/low-L regime, the trend changes and the theoretical prediction significantly underestimates the measured $\langle v_z \rangle$. Thus, unsurprisingly, the theory fails outside of the applicable regime.

Figures 13(a) and 13(b) show simulation results for $\langle v_z \rangle$ for $N=17$ and $N=25$, respectively, with theoretical predictions overlaid on the simulation data. Only results for $t_{\mathrm{off}}=20$ are shown. In each case, the theory gives reasonable predictions for $\langle v_z \rangle$ in the low-N/high-L regime and diverges considerably from the simulation results at lower L where the system falls outside this regime.

The simple theoretical model described in this section builds on that employed in the experimental studies of Refs. [4–6]. Our theoretical description was shown to give a reasonable prediction of the velocity in the regime where center-of-mass diffusion is expected to be significant. This regime is identifiable from the nature of the dependence of $\langle v_z \rangle$ and β_z with N and L, as discussed in Secs. III A and III B, respectively. Thus, the results in this section strongly support the interpretation of the data in those sections.

F. High-*N*/low-*L* regime

From the results presented in Secs. III A and III B above, we argued that there are two distinct dynamical regimes. When the polymer size is sufficiently small relative to L, center-of-mass diffusion is an important component of the motional mechanism of the polymer in the ratchet. The simple theoretical model developed in Sec. III E was helpful in providing some understanding of the dynamical behavior in this regime. For example, it explains the N dependence of $\langle v_z \rangle$, and why HD interactions increase the rate of transport. As noted earlier, the dynamical behavior in the high-N/low-L regime is somewhat different. While HD interactions do also increase $\langle v_z \rangle$, as in the low-N/high-L case, this regime is distinguished by the fact that $\langle v_z \rangle$ is insensitive to changes in N, as well the fact that β_z increases with decreasing L. Obviously, a complete picture of the dynamics of the polymer/ratchet system needs to address these observations. In Sec. III B, it was argued that the dominant motional mechanism in this regime involves the coupling of the internal degrees

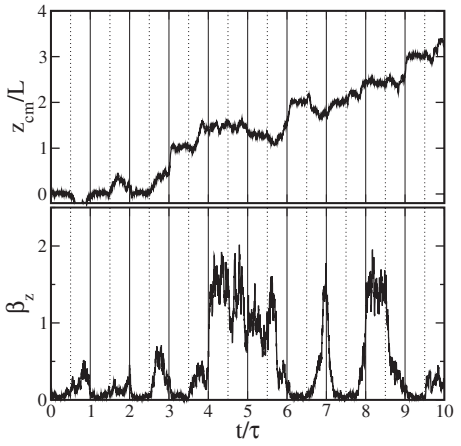

FIG. 14. Time dependence of scaled polymer center-of-mass position, z_{cm} (top), and deformation factor, β_z (bottom), over ten cycles of the flashing ratchet. Data are shown for a polymer of length $N=25$ in a ratchet of length $L=10$. HD interactions are present. Solid vertical grid lines indicate times when the ratchet potential is turned on and dotted grid lines indicate times when the potential is turned off.

of freedom to the cycling of the ratchet potential. While we do not provide a quantitative theoretical analysis of the motion in this regime in this study, we present a few results that illustrate the nature of this coupling and that could be helpful in developing a theoretical model to account for the observed trends.

Figure 14 shows the time dependence of z_{cm} and β_z over a single simulation for a polymer of length $N=25$ in a ratchet with $L=10$ and for $t_{on}=t_{off}=20$. HD interactions are present. Inspection of Figs. 2(b) and 3(a) shows that this corresponds to the high-N/low-L regime. Over the 10 ratchet cycles shown in the figure, the polymer moves roughly three ratchet periods. A stepping event is evident when the ratchet is toggled on at $t/\tau=3$. Immediate before and after the event, the polymer remains highly flattened with some conformational relaxation in the off-phase immediately prior to the event. Thus, the whole polymer jumps from one ratchet minimum to the next in one ratchet cycle. This is by far the dominant type of stepping event in the low-N/high-L regime. However, in the high-N/low-L regime, this type of stepping event is the exception and becomes increasingly rare as N increases and/or L decreases. Over two ratchet cycles during $t/\tau=4-6$, the polymer undergoes a more prolonged stepping event accompanied by a conformational expansion along the z axis. Clearly, the monomers remain distributed over at least two ratchet periods during this phase, as different portions of the polymer are attracted to different potential minima. Conformational fluctuations during the off-phase will enable a greater portion of the polymer to become captured by the next minimum the next time the ratchet is turned on. In this way, the coupling of the internal dynamics of the chain to the ratchet becomes a significant part of the motional mechanism. Another similar stepping event, characterized by a stretched chain during at the on-phase over at least one complete cycle, is evident in the interval $t/\tau=8-9$. As N increases and/or L decreases, the frequency of these multicycle stepping events increases. In addition, the time between the

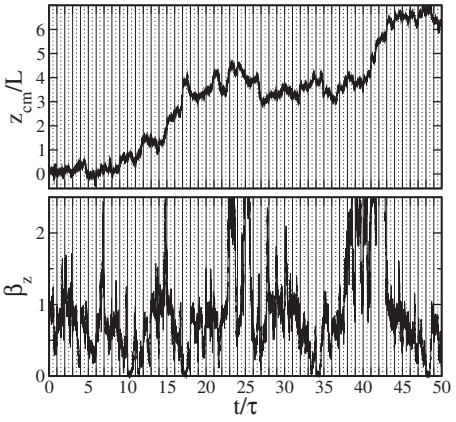

FIG. 15. As in Fig. 14, except for $N=50$ and $L=6$.

events decreases, eventually to the point where individual stepping events can no longer be defined. Figure 15 illustrates such a case for a $N=50$ polymer and a ratchet length of $L=6$. Unlike the case shown in Fig. 14, the polymer is rarely in the highly flattened state, as characterized by a very low β_z, which divides discrete stepping events. Rather, the behavior of β_z indicates that the polymer remains extended along the ratchet axis, and thus remains stretched over multiple potential wells over its trajectory. This trend corresponds to the increase in the average β_z with decreasing L and increasing N shown in Fig. 3.

These results clearly demonstrate the connection between conformational fluctuations and polymer transport in the high-N/low-L regime. The efficiency of this mechanism for driving polymer transport is expected to be correlated with the fluctuation rate. Since incorporation of HD interactions increases the rate of these fluctuations, the polymer velocity increases correspondingly. This is analogous to the effect that HD interactions enhance the rate of diffusion and, thus, increase the velocity in the low-N/high-L regime.

IV. SUMMARY AND CONCLUSIONS

In this paper, we have used Brownian dynamics simulations to examine the dynamical behavior of a model polymer subject to the action of a flashing ratchet potential. The average speed of the polymer and its conformational behavior have been examined upon variation in the polymer length and ratchet spatial period. This work builds on an earlier simulation study by Downton *et al.*, [8] which investigated a similar model system. An important addition to the model in the present paper is the incorporation of HD effects. These HD interactions were incorporated using the RPY diffusion tensor [42,43] and the Ermak and McCammon simulation method [46], in contrast to another recent study which investigated HD effects on a polymer Brownian motor by employing an explicit solvent. [9] The approach used in this study has the advantage of computational efficiency and provides a straightforward means to compare the HD and non-HD cases. In addition to adding HD, we have extended the range of polymer lengths considered in Ref. [8].

As observed in Ref. [8], we find that the velocity of the polymer in the Brownian ratchet exhibits a single maximum

upon variation with respect to L for each chain length, N. For otherwise identical systems, HD interactions always have the effect of increasing the polymer velocity. The simulation results indicate that there are two distinct dynamical regimes: (1) a low-N/high-L regime in which the velocity decreases appreciably with increasing N and (2) a high-N/low-L regime in which the velocity is insensitive to variations in N. The regimes exist for both HD and non-HD systems. The transport behavior is correlated with the conformational behavior of the polymer, which is quantified by the deformation factor, β_z, a measure of the ratchet-induced compression or expansion of the polymer. In the low-N/high-L regime, β_z increases slightly with increasing L, while in the high-N/low-L regime, β_z increases sharply with decreasing L. The value of the ratchet length L at the minimum of β_z corresponds closely the transition between the regimes in the velocity. Incorporation of HD interactions and variation in t_{off} each shift the location of the transition in predictable ways. The origin of these trends relates to the degree of conformational relaxation of the polymer during the off-phase, which depends on the ratio $t_{\mathrm{off}}/\tau_{\mathrm{r}}$, where τ_{r} is the longest relaxation time of the internal modes for a polymer in equilibrium.

The dominant mode of transport in the low-N/high-L regime involves center-of-mass diffusion of the polymer. In this regime, the polymer position is advanced in discrete steps over a single ratchet cycle, and the polymer typically assumes an oblate shape with the monomers completely localized over a distance L between two adjacent potential maxima when the ratchet potential is on. For this case, we developed a theoretical description by building on an even simpler theoretical model [49] that had been applied in the analysis of experimental data. Our model removed three simplifying approximations of the original version and yielded significantly better quantitative predictions of the polymer velocity in the low-N/high-L regime defined by the behavior of the velocity and β_z. This description clearly accounts for the increase in the velocity with decreasing N and with the incorporation of HD interactions in terms of increasing the diffusion rate of the polymer. Since the theoretical model uses simulation data as input, it is of limited use for quantitative predictions in experimental systems. However, it does provide a very helpful means of confirming the nature of the motional mechanism for this regime.

In the regime of high-N/low-L, the dominant motional mechanism involves a coupling of the internal dynamical modes of the polymer to the cycling of the ratchet potential. Where they can be distinguished, stepping events typically occur over multiple time cycles of the ratchet during which the polymer is stretched over two or more spatial ratchet periods. We did not present a theoretical model to account for the observed trends. Nevertheless, our observations do at least suggest that the larger velocity observed for the HD system arises from the corresponding increase in the rate of shape fluctuations.

The main motivation for the present simulation study lies in its relevance to the development of technological applications employing Brownian ratchets. One important application is the transport and size-based separation of biopolymers, such as that described in Refs. [4–6], in which transport and separation of charged DNA fragments were achieved using a micromachined device employing interdigitated electrodes to produce a ratchet potential. Insights gained from simulation studies of simple polymer/ratchet model systems could be helpful in guiding the development of such applications. The present paper builds on the simulation work of Downton *et al.* [8] by incorporating HD effects into the molecular model; these effects are expected to significant for transport of DNA fragments in aqueous solution. In addition, our study complements the recent work of Kenward and Slater [9] by demonstrating that the impact of ratchet-induced polymer shape deformations on the drift velocity observed for the explicit-solvent model used in Ref. [9] can also be probed using a more computationally efficient implicit-solvent model.

An important contribution of the present work is the elucidation of the different regimes corresponding to different motional mechanisms. The very weak dependence of the polymer velocity on chain length observed in Ref. [8] for the non-HD system corresponded to one of these dynamical regimes. In the other regime, where center-of-mass diffusion is a key component of the transport mode, the dependence of the velocity on chain length is pronounced. Our analysis of the results should be helpful in predicting the location of the latter regime, where size-based separation is feasible, using known properties of a polymer in equilibrium.

While this work provides useful insights into the behavior of polymers in Brownian ratchets, the nature of the model employed imposes limitations on its relevance to experimental systems. For example, with regard to device studied in Refs. [4–6], the ratchet potential arises from electrostatic interaction between the DNA fragment and electrodes of finite width mounted on a surface. Using the one-dimensional ratchet potential of Eq. (6) is a highly simplified representation of the system. A realistic three-dimensional model would necessarily incorporate polymer-surface interactions, including surface effects on HD interactions. The coupling between the conformational and dynamical behavior for such a model is expected to more complex. A more straightforward extension to the model would be use of a semiflexible chain model with a tunable persistence length; such a model could be highly relevant to understand the behavior of very short DNA fragments, as noted in Ref. [6].

ACKNOWLEDGMENTS

This work was supported by the National Research Council of Canada (NSERC) and by the Canada Foundation for Innovation (CFI). We are grateful to WestGrid and to the Atlantic Computer Excellence Network (ACEnet) for use of their computational facilities.

[1] J. Fu, P. Mao, and J. Han, Trends Biotechnol. **26**, 311 (2008).
[2] G. B. Salieb-Beugelaar, K. D. Dorfman, A. van den Berg, and J. C. T. Eijkel, Lab Chip **9**, 2508 (2009).
[3] G. W. Slater *et al.*, Electrophoresis **30**, 792 (2009).
[4] J. Bader, R. W. Hammond, S. A. Henck, M. W. Deem, G. A. McDermott, J. M. Bustillo, J. W. Simpson, G. T. Mulhern, and J. M. Rothberg, Proc. Natl. Acad. Sci. U.S.A. **96**, 13165 (1999).
[5] R. W. Hammond, J. S. Bader, S. A. Henck, M. W. Deem, G. A. McDermott, J. M. Bustillo, and J. M. Rothberg, Electrophoresis **21**, 74 (2000).
[6] J. S. Bader, M. W. Deem, R. W. Hammond, S. A. Henck, J. W. Simpson, and J. M. Rothberg, Appl. Phys. A: Mater. Sci. Process. **75**, 275 (2002).
[7] H. Linke, M. T. Downton, and M. J. Zuckermann, Chaos **15**, 026111 (2005).
[8] M. T. Downton, M. J. Zuckermann, E. M. Craig, M. Plischke, and H. Linke, Phys. Rev. E **73**, 011909 (2006).
[9] M. Kenward and G. W. Slater, Phys. Rev. E **78**, 051806 (2008).
[10] E. R. Kay, D. A. Leigh, and F. Zerbetto, Angew. Chem., Int. Ed. **46**, 72 (2007).
[11] Y. Zhang and J. Chen, Physica A **387**, 3443 (2008).
[12] A. Grillo, A. Jinha, S. Federico, R. Ait-Haddou, W. Herzog, and G. Giaquinta, J. Phys. A **41**, 015002 (2008).
[13] Z. Wang, Proc. Natl. Acad. Sci. U.S.A. **104**, 17921 (2007).
[14] K. Yamano, M. Kuroyanagi-Hasegawa, M. Esaki, M. Yokota, and T. Endo, J. Bio. Chem. **283**, 27325 (2008).
[15] H. Hagman, C. M. Dion, P. Sjölund, S. J. H. Petra, and A. Kastberg, EPL **81**, 33001 (2008).
[16] P. Sjölund, S. J. H. Petra, C. M. Dion, H. Hagman, S. Jonsell, and A. Kastberg, Eur. Phys. J. D **44**, 381 (2007).
[17] P. Sjölund, S. J. H. Petra, C. M. Dion, S. Jonsell, M. Nylén, L. Sanchez-Palencia, and A. Kastberg, Phys. Rev. Lett. **96**, 190602 (2006).
[18] M. Schiavoni, L. Sanchez-Palencia, F. Renzoni, and G. Grynberg, Phys. Rev. Lett. **90**, 094101 (2003).
[19] L. Sanchez-Palencia, Phys. Rev. E **70**, 011102 (2004).
[20] W. R. Browne and B. L. Feringa, Nat. Nanotechnol. **1**, 25 (2006).
[21] P. Palffy-Muhoray, T. Kosa, and E. Weinan, Appl. Phys. A: Mater. Sci. Process. **75**, 293 (2002).
[22] P. Hänggi, F. Marchesoni, and F. Nori, Ann. Phys. (Leipzig) **14**, 51 (2005).
[23] P. Reimann and P. Hänggi, Appl. Phys. A: Mater. Sci. Process. **75**, 169 (2002).
[24] E. M. Craig, M. J. Zuckermann, and H. Linke, Phys. Rev. E **73**, 051106 (2006).
[25] S. von Gehlen, M. Evstigneev, and P. Reimann, Phys. Rev. E **77**, 031136 (2008).
[26] M. Bier, BioSystems **93**, 23 (2008).
[27] Y. Ishii, Y. Taniguchi, M. Iwaki, and T. Yanagida, BioSystems **93**, 34 (2008).
[28] R. D. Astumian, BioSystems **93**, 8 (2008).
[29] D. Kinderlehrer and M. Kowalczyk, Arch. Ration. Mech. Anal. **161**, 149 (2002).
[30] H. Qian, J. Math. Chem. **27**, 219 (2000).
[31] E. M. Craig, N. J. Kuwanda, B. J. Lopez, and H. Linke, Ann. Phys. (Berlin) **17**, 115 (2008).
[32] D. Suzuki and T. Munakata, Phys. Rev. E **68**, 021906 (2003).
[33] T. Yanagida, BioSystems **93**, 3 (2008).
[34] D. Li, D. Fan, and Z. Wang, J. Chem. Phys. **126**, 245105 (2007).
[35] R. Krishnan, D. Dan, and A. M. Jayannavar, Physica A **354**, 171 (2005).
[36] V. M. Rozenbaum, T. Y. Korochkova, and K. K. Liang, Phys. Rev. E **75**, 061115 (2007).
[37] J. Kauttonen, J. Merikoski, and O. Pulkkinen, Phys. Rev. E **77**, 061131 (2008).
[38] R. F. Fox and M. H. Choi, Phys. Rev. E **63**, 051901 (2001).
[39] A. Houdusse and H. L. Sweeney, Curr. Opin. Struct. Biol. **11**, 182 (2001).
[40] T. Yanagida, S. Esaki, A. H. Iwane, Y. Inoue, A. Ishijima, K. Kitamura, H. Tanaka, and M. Tokunaga, Philos. Trans. R. Soc. London, Ser. B **355**, 441 (2000).
[41] T. C. Elston and C. S. Peskin, SIAM J. Appl. Math. **60**, 842 (2000).
[42] J. Rotne and S. Prager, J. Chem. Phys. **50**, 4831 (1969).
[43] H. Yamakawa, J. Chem. Phys. **53**, 436 (1970).
[44] D. Houtman, I. Pagonabarraga, C. P. Lowe A. Esseling-Ozdoba3, A. M. C. Emons, and E. Eiser, EPL **78**, 18001 (2007).
[45] J. A. Fornés, J. Colloid Interface Sci. **341**, 376 (2010).
[46] D. L. Ermak and J. A. McCammon, J. Chem. Phys. **69**, 1352 (1978).
[47] The simulation method used in the study of Ref. [8] involved the numerical integration of the Langevin equation with the inertial term included. The method employed in the present paper uses instead the overdamped Langevin equation; i.e., we neglect the inertial term. The numerical integration method of Ref. [46] required for HD simulations is built on this approximation. Using the overdamped Langevin equation enables a more straightforward comparison between the HD and non-HD systems.
[48] M. Doi and S. F. Edwards, *The Theory of Polymer Dynamics*, International Series of Monographs on Physics (Oxford University Press, Oxford, 1986), Vol. 73.
[49] A. Ajdari and J. Prost, C. R. Acad. Sci., Paris II **315**, 1635 (1992).